

Synthesis and Size-Dependent Properties of [12], [16], and [24]Carbon Nanobelts

Guillaume Povie,^{†,‡} Yasutomo Segawa,^{*,†,‡} Taishi Nishihara,^{†,‡} Yuhei Miyauchi,^{†,‡,§} and Kenichiro Itami^{*,†,‡,¶}

[†]JST-ERATO, Itami Molecular Nanocarbon Project, Nagoya University, Chikusa, Nagoya 464-8602, Japan

[‡]Graduate School of Science, Nagoya University, Chikusa, Nagoya 464-8602, Japan

[§]Institute of Advanced Energy, Kyoto University, Uji, Kyoto, 611-0011, Japan

[¶]Institute of Transformative Bio-Molecules (WPI-ITbM), Nagoya University, Chikusa, Nagoya 464-8602, Japan

ABSTRACT: The synthesis and X-ray crystal structure of the first member of the carbon nanobelt family is reported. [12]carbon nanobelt ([12]CNB) was originally obtained from a nickel-mediated reductive coupling reaction of a dodecabrominated macrocyclic precursor, albeit only in 1% yield. The present article reports on the development of this synthetic strategy and its extension to the preparation of the [16] and [24]CNB analogues. In particular, our extensive investigations on the final belt-forming, nickel-mediated reaction led to the development of a new ligand system that provides [12]CNB in up to 7% yield, contributing to the commercialization of [12]CNB. The belt structures of [12], [16], and [24]CNB were characterized by NMR, UV-vis, and Raman spectroscopy as well as mass spectrometry and X-ray crystallography. The fluorescence of the CNBs in solution displayed a remarkable dependence on the ring size, ranging from a broad red emission ([12]CNB) to a narrow-band blue emission ([24]CNB), while both features are observed for [16]CNB.

Introduction

The size- and structure-selective synthesis of carbon nanotubes (CNTs; Figure 1a) remains a long-standing target in nanocarbon science. Since the first observation and structural analysis of CNTs in 1991 by Iijima,¹ the synthesis of CNTs has been of much interest owing to their outstanding physical and electronic properties, which depend on their size and structures.² Although a wide range of methods such as arc evaporation, laser ablation, and chemical vapor deposition have been reported for the synthesis of CNTs,^{3a} synthetic methods that offer perfect control over the structure of CNTs^{3b} remain a fundamental bottleneck to the progress of CNT-based material sciences.

The bottom-up organic synthesis of CNT structures could potentially be used to solve this problem. As the first step toward the ultimate goal, cylindrical polyaromatic molecules that represent the side-wall segment of CNTs have received substantial attention.⁴ These carbon nanorings and carbon nanobelts (CNBs)⁵ had been targeted by synthetic chemists even before the discovery of CNTs. Carbon nanorings, *i.e.*, linked arene systems that are represented by [*n*]cycloparaphenylenes ([*n*]CPPs; Figure 1a) have been targeted by synthetic chemists since the 1930s,⁶ and meanwhile, a variety of such carbon nanorings have been synthesized using “strain-releasing” strategies originally reported by the groups of Jasti, Itami, and Yamago.^{4,7} Since the development of a size-selective method to synthesize [*n*]CPPs (*n* = 5-18), their size-dependent features such as unusual photophysical properties,⁸ reactivity,⁹ host-guest interactions,¹⁰ and the potential utility for CNT growth¹¹ have been revealed.

In contrast, the synthesis of CNBs had not been accomplished until very recently. The first mentioning of [12]cyclacene as a

cylindrical strip of fused benzene rings (CNBs) dates back to the 1950s (Figure 1a).¹² In a visionary postface published in 1983, Vögtle proposed the structure of an armchair-type CNB that would later be named Vögtle belt (Figure 1a).¹³ The following years witnessed several studies aimed at the synthesis of CNBs.¹⁴ Over the years, several belt-shaped structures consisting of sp²-carbon atoms were prepared either by incorporating bent cyclooctatetraene units to accommodate the strain,¹⁵ or by derivatization of fullerenes to reproduce the π-system of [10]cyclophenacene.¹⁶ In parallel, Scott and co-workers demonstrated the possibility to generate related structures in a controlled fashion using pyrolytic technics, culminating in the assembly of an endcap structure of (5,5)CNT.¹⁷ Yet, despite numerous attempts toward the synthesis of cyclacene and its derivatives¹⁸ as well as armchair-type structures,¹⁹ the synthesis of a genuine CNB has remained elusive.

With the advent of CPP chemistry over the past decade, the synthesis of CNBs seemed closer than ever. However, most efforts toward the π-extension of the aromatic system were met with strain-relieving rearrangements that disrupted the cylindrical shape.^{19c,20} Jasti and co-workers have prepared a partially fused structure from alkenyl-substituted CPPs using olefin metathesis (Figure 1b),^{19g} but the difficulty associated with accessing the required fully functionalized CPPs has so far prevented the formation of CNBs via this strategy.²¹ Facing similar issues, we decided to use a flexible cyclophane based on *Z*-alkene bridges instead. In light of Iyoda's attempt at generating [10]cyclophenacene by the oxidative photocyclization of a non-substituted benzannulene (Figure 1c),^{19f} we investigated the possibility to carry out a similar transformation under reductive conditions using a suitably functionalized starting material.

Following this approach, we have reported the preparation of the polybrominated macrocycle **4** and its transformation into the [12]CNB (**1**) upon reaction with a Ni(cod)₂/2,2'-bipyridyl complex, albeit that **1** was obtained in merely 1% yield.²² Herein, we report on the reexamination of some key aspects of this synthetic route and its extension to the preparation of the larger nanobelt analogues [16]CNB (**2**) and [24]CNB (**3**) (Figure 1d). The photophysical properties of this series of compounds were analyzed in detail and rationalized based on the results of DFT calculations.

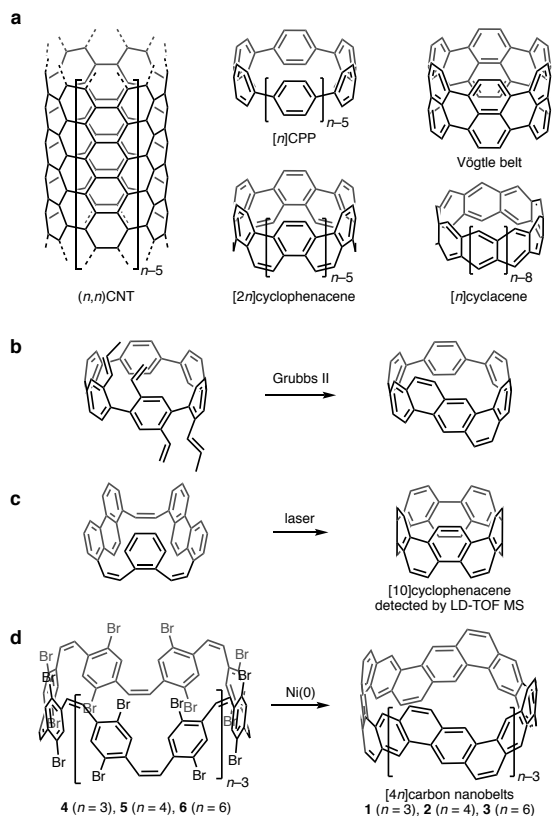


Figure 1. a) Structures of CNTs, CPPs, and representative CNBs. b) The π -extension of CPPs using olefin metathesis. c) Detection of [10]cyclophenacene by LD-TOF MS. d) Synthesis of [12], [16], and [24]CNBs (this work).

Results and Discussion

Synthesis

The synthetic route to CNBs **2** and **3** is summarized in Scheme 1. The synthesis of the macrocyclic belt precursors is based on Wittig reactions between unsymmetrical 2,5-dibromo-*p*-xylene derivatives, taking advantage of the high *Z*-selectivity induced by the *ortho*-halogen substituents.²³ A key feature for this synthetic route was the serendipitous discovery of an efficient desymmetrization reaction of readily accessible hexabromo-*p*-xylene.²⁴ Treating **7** with sodium methanolate in a biphasic toluene/methanol solution unexpectedly furnished monoacetal **9** in high yield instead of the corresponding diacetal (for details, see SI). Starting from **9**, an iterative deprotection/Wittig reaction provided trimer **16**²² and tetramer **17** in high yield, albeit that further homologation was hampered by the prohibitively low solubility of the pentamer.

Instead, we resorted to a one-shot oligomerization-macrocyclization. The required bifunctional units were readily prepared upon reaction with PPh₃, followed by deprotection of the aldehyde under acidic conditions, and crystallization as the hexafluorophosphate (**18**) in 46% yield from **14**.

As originally reported,²² the cyclic hexamer **4** was the main product of the reaction between the bifunctional trimer with *t*-BuOK, while the cyclic trimer was not detected. In contrast, tetramer **18** underwent smooth cyclization to afford cyclic tetramer **19** in 20–40% yield as a mixture of *Z,Z,Z,Z,Z,Z*- and *Z,Z,Z,Z,E*-isomers under similar conditions, *i.e.*, upon reaction with *t*-BuOK under moderately diluted conditions (10–40 mM). Reverse addition conditions afforded very poor results with *t*-BuOK, but the use of DBU in trichloroethylene increased the yield of **19** to 60%. Under these conditions, 11% of the cyclic octamer **5** could also be isolated, albeit in a 2:1 ratio with the *Z,Z,Z,Z,Z,Z,Z,Z,E*-isomer. To favor the formation of larger macrocycles, we attempted the oligomerization of **18** in concentrated CH₂Cl₂ solutions using *t*-BuOK. Despite their very low solubility, the resulting higher-order oligomers could be dissolved in boiling 1,1,2,2-tetrachloroethane, before they were slowly added to the mixture to carry out the macrocyclization step at low concentrations. Under these conditions, cyclic octamer **5** and dodecamer **6** were obtained in ~15% and 3% yield, respectively, including their *E*-isomers. Both **5** and **6** were thus preferentially used without complete isolation in the final belt-forming, nickel-mediated coupling reaction, and accurate yields were calculated over two steps from **18**.

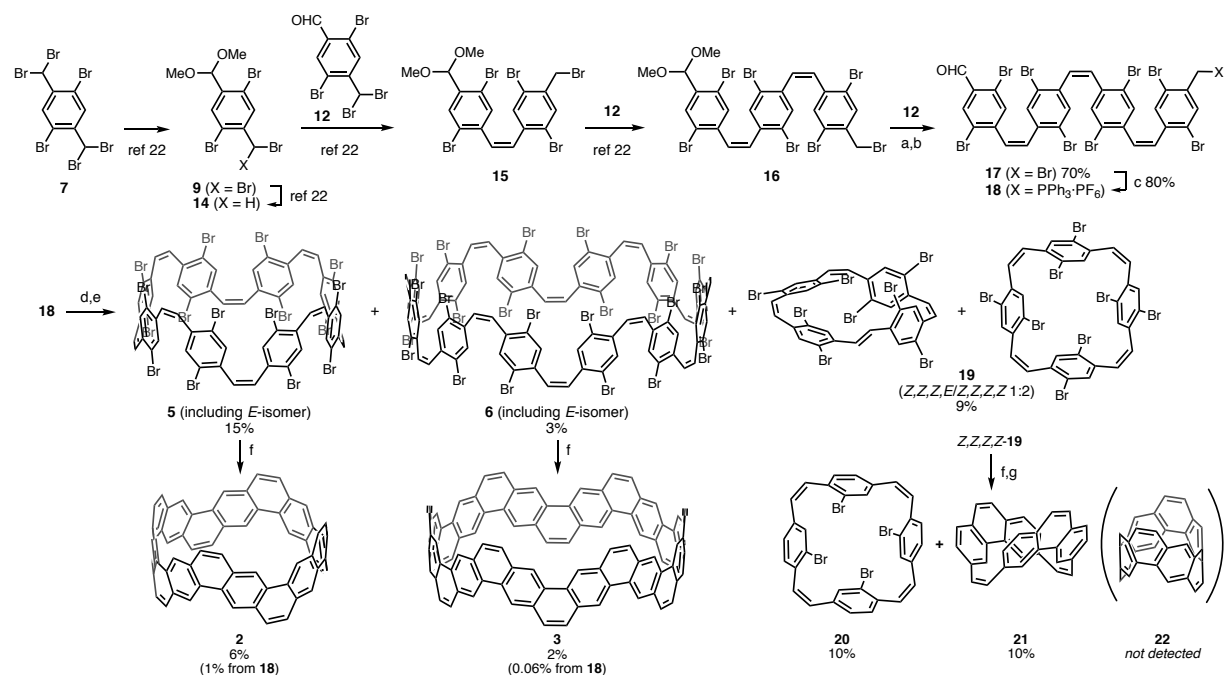
Table 1. Ligand effects on the Ni(0)-mediated formation of **1**.^a

Entry	Ligand		yield (%) ^b
	X	Y	
1 ^c	H	H	1.5
2	H	H	0.5
3	Me	H	0.5
4	H	Me	0.5
5	OMe	H	0.1
6	CF ₃	H	2.0
7	CO ₂ Me	H	1.0
8	H	CF ₃	4.0
9	H	CO ₂ Me	7.0 (5.0) ^d

^a 10 μ mol of **4**, 12 equiv of Ni(cod)₂/ligand, DMA/toluene, 75 °C, 2 h unless otherwise noted. ^b ¹H NMR yield using *i*-PrOH as the internal standard. ^c Reaction stopped after 15 min. ^d Isolated yield.

Originally, [12]CNB (**1**) was obtained from macrocycle **4** using a standard combination of Ni(cod)₂ and 2,2'-bipyridyl.^{22,25} However, the very low yield, which further decreased with prolonging the reaction time (Table 1, entry 2), led us to conclude that **1** may be unstable under these conditions. Indeed, after treating a pure sample of **1** with an excess of the Ni(cod)₂/2,2'-bipyridyl in DMA at 75 °C, we recovered only 20% of **1** and other products were not detected after the usual workup.

Scheme 1. Synthesis of CNBs **2** and **3**.



Reaction conditions: a) PPh_3 (1.04 equiv), THF/MeOH, reflux, 3 h; then **12** (1.02 equiv), $t\text{-BuOK}$ (1 M in THF, 1.00 equiv), rt, 30 min; b) $(\text{MeO})_2\text{POH}$ (1.30 equiv), $i\text{-Pr}_2\text{NEt}$ (1.40 equiv), rt, 3–6 h; c) PPh_3 (1.04 equiv), THF/MeOH, reflux, 5 h; 4 M aq. HCl, acetone, rt, 9 h, then KPF_6 , CH_2Cl_2 , rt, 3 min; d) $t\text{-BuOK}$ (0.3 equiv), CH_2Cl_2 , rt, 10 min, repeated five times; e) $\text{Cl}_2\text{CHCHCl}_2$, 140 °C, then KOH (100 equiv), $\text{CH}_2\text{Cl}_2/\text{EtOH}$, 0 °C, 3 h; f) $\text{Ni}(\text{cod})_2/5,5'$ -bis(methoxycarbonyl)-2,2'-bipyridyl (**5**: 16 equiv; **6**: 25 equiv; **19**: 8.5 equiv), DMA/toluene, 75 °C, 30 min. g) TFA (50 equiv), 75 °C, 30 min.

Speculating that a lower electron density at the nickel center might both decrease its ability to decompose **1** and favor the strain-inducing reductive elimination to produce **1**, we investigated the ligand effects. After screening the 2,2'-bipyridyl derivatives bearing electron-donating groups (Me, OMe; entries 3–5) or -withdrawing groups (CF_3 , CO_2Me ; entries 6–9), we discovered that 5,5'-bis(methoxycarbonyl)-2,2'-bipyridyl afforded an NMR yield of 7% and an isolated yield of 5% after recrystallization from THF. Submitting cyclic octamer **5** and dodecamer **6** to these reaction conditions furnished the corresponding [16]CNB (**2**) and [24]CNB (**3**) in 1% and 0.06% yield from **18**, respectively. Reaction of the cyclic tetramer (*Z,Z,Z,Z*)-**19** was also attempted. Although a product could not be identified after applying the homocoupling conditions, further treatment of the reaction mixture with trifluoroacetic acid (TFA) furnished tetradebrominated product **20**, which was confirmed by X-ray crystallography, and phenanthrenophanediene **21**. The [8]CNB **22** was not observed probably due to its extremely high strain energy ($179 \text{ kcal}\cdot\text{mol}^{-1}$).⁵

X-ray crystal structures

Crystals of **1**·2THF were obtained as red chamfered cubes upon evaporation of a $\text{CH}_2\text{Cl}_2/\text{THF}$ solution of **1**. An X-ray diffraction analysis revealed that the CNBs are arranged in a cubic system, in which one molecule of THF sits above each CNB cavity and one below. Similar to the previously described 1.3CHCl_3 ,²² **1** displays a virtually flawless circular shape with a diameter of ca. 8.3 Å (Figure 2a). Crystals of **2** suitable for X-ray crystallography were obtained from the slow diffusion of *n*-hexane into a solution of **2** in benzene

and 1,1,2-trichloroethylene, whereby the solvents were incorporated in the crystal structure in a highly disordered fashion. Although two crystallographically distinct CNBs are contained within the unit cell, both display similar structural features with a disordered benzene molecule located in the cavity and an elliptic deformation of the cylindrical shape (Figure 2b). A low-resolution X-ray structure of crystals of **3** grown upon diffusion of cyclohexane into a $\text{CHCl}_3/\text{CS}_2$ solution of **3** was also determined. In these crystals, the CNBs assemble in a hexagonal lattice, creating an additional pore in the structure. [24]CNB (**3**) also exhibits an elliptic deformation in the crystal structure, with a difference of more than 2 Å between the long and short axis of the ellipse (Figure 2c). The deformation of the cylindrical shape in the crystal structures of [16]CNB and [24]CNB indicates that these compounds remain flexible.

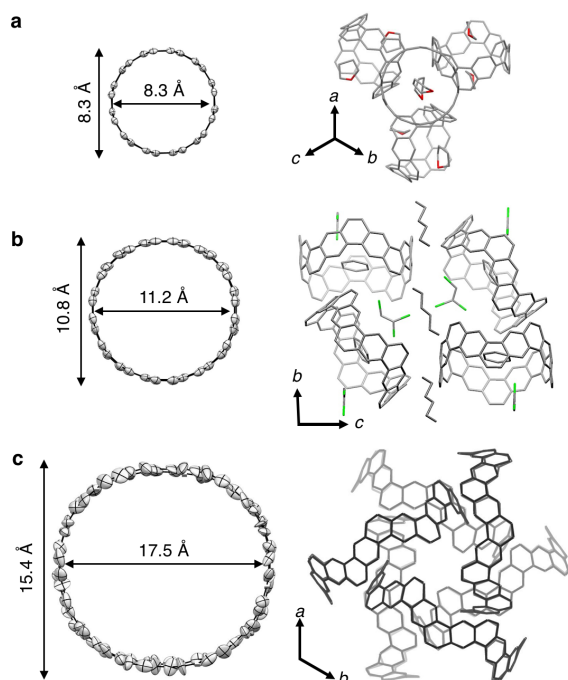


Figure 2. X-ray crystal structures of (a) 1-2THF (packing structure viewed perpendicular to the (111) plane); (b) **2** (packing structure viewed along the *a* axis); (c) **3** (packing structure viewed along the *c* axis); all ORTEPs are shown at 50% probability with hydrogen atoms and solvent molecules omitted for clarity. The shortest and longest distances (in Å) between opposite carbon atoms of the central part of

the rings are shown.

Photophysical properties

To probe the effect of the ring size on the electronic structure of the CNBs, their photophysical properties in solution were investigated. The UV-vis absorption spectra of **2** and **3** in CH_2Cl_2 show patterns similar to that previously reported for **1**: 1) a strongly absorbing region below 400 nm, whereby **2** shows clear maxima; 2) a weaker absorption extending up to 450–500 nm including clearly resolved bands (Figures 3a-c). The maximum absorption wavelength of the spectra undergoes a bathochromic shift with increasing ring size from 313 nm (**1**) to 333 nm (**2**), and further splitting of the two resolved bands at 351 and 356 nm for **3**. In contrast, the weakly absorbing region experiences a hypsochromic shift with increasing ring size: 496 nm (**1**), 478 nm (**2**), and 466 nm (**3**). The resolved bands of all CNBs in the longer wavelength-absorbing region should be attributed to the symmetry allowed transitions with weak oscillator strength (**1**: $f_{0-0} = 0.0053$; **2**: $f_{0-0} = 0.0076$; **3**: $f_{0-0} = 0.0136$) that can be predicted based on time-dependent density functional theory (TD-DFT). The resolved band of **3** corresponds to the $S_0 \rightarrow S_1$ transition (HOMO \rightarrow LUMO), while those of **1** and **2** are the $S_0 \rightarrow S_2$ transition (HOMO-1 \rightarrow LUMO/HOMO \rightarrow LUMO+1). The $S_0 \rightarrow S_1$ transitions of **1** and **2** are symmetry forbidden and may possibly be located around the resolved bands as small broadened bands.

The fluorescence spectra show a more singular size dependence. Upon excitation at 350 nm, **2** displays a broad green emission band centered at 524 nm with a shoulder at 563 nm that further extends up to 650 nm. Although the general shape of the latter feature

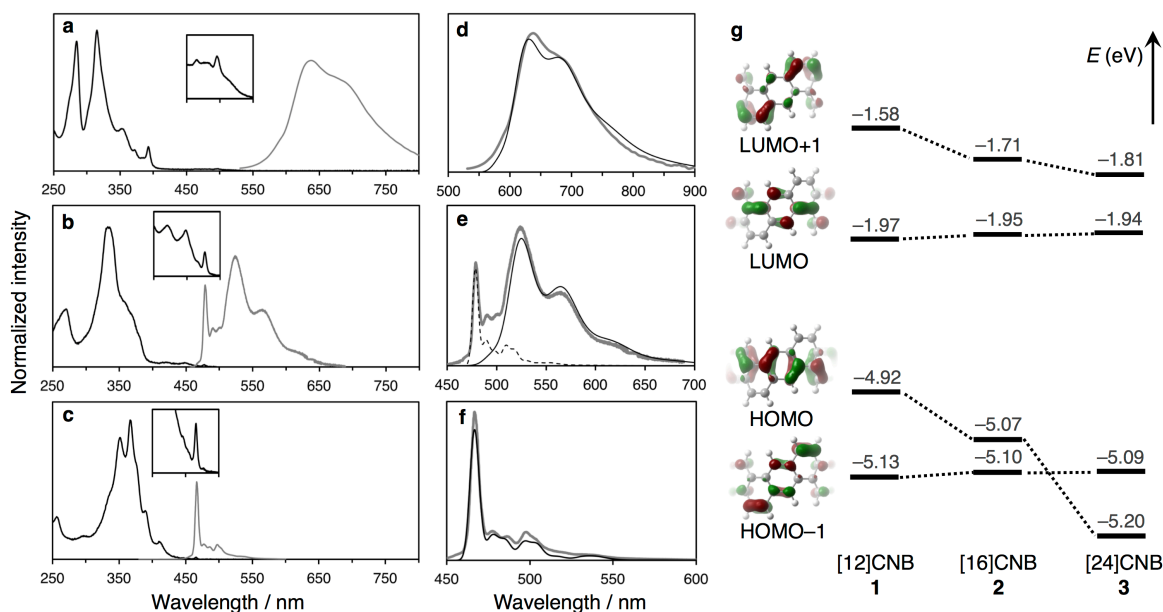


Figure 3. UV-visible absorption (black line) and fluorescence (grey line) spectra of CH_2Cl_2 solutions of **1** (a), **2** (b), and **3** (c). The insets show magnifications of the weakly absorbing region (using an abscissa scale that is identical to that of the main plot). Fluorescence spectra were recorded upon excitation at 500 nm (**1**), 360 nm (**2**) and 367 nm (**3**). Experimental fluorescence spectra (grey lines) compared to the results of Frank-Condon Hertzberg-Teller calculations for the $S_0 \leftarrow S_1$ (plain black line) transition of **1** (d), the $S_0 \leftarrow S_1$ (plain black line) and $S_0 \leftarrow S_2$ (dotted black line) transitions of **2** (e), and the $S_0 \leftarrow S_1$ (plain black line) transition of **3** (f). (g) Energetic diagram of the frontier molecular orbitals of **1**, **2**, and **3** in the ground state calculated at the B3LYP/6-31G(d) level of theory. Dotted lines link orbitals with identical symmetry. The orbital distributions are illustrated using one repeat unit of **1** (isovalue = 0.03).

closely resembles the red emission of **1** (550–850 nm, $\lambda_{\text{max}} = 635$ nm), **2** also exhibits an additional sharp band at 478 nm. The sharp fluorescence band is the characteristic component of the spectrum for **3** ($\lambda_{\text{max}} = 466$ nm), with only minor vibrationally-resolved signals up to 550 nm. The wavelengths of the sharp fluorescence bands of **2** and **3** agree with those of the observed peaks in the absorption. Thus, it is reasonable to consider that the sharp fluorescence bands represent the zero-Stokes shift emissions of the corresponding symmetry allowed transitions; $S_0 \leftarrow S_2$ of **2** and $S_0 \leftarrow S_1$ of **3**. For **2**, the broad emission centered at 524 nm should be assigned to the $S_0 \leftarrow S_1$ transition. The origin of these fluorescence properties of **2** can be explained in terms of the thermal population of the S_2 energy level; when the energy difference between the S_1 and S_2 levels is smaller than or comparable to the thermal energy at room temperature, radiative decay processes can occur simultaneously from the S_1 and S_2 levels.^{26,27} The validity of this hypothesis was confirmed by the fluorescence spectrum of **2** in a polymer matrix recorded at 10 K (see SI). The sharp fluorescence of **2** was virtually absent, suggesting that only the broad $S_0 \leftarrow S_1$ transition occurs given that the S_2 energy level cannot be populated thermally.

The emission properties of the CNBs were further investigated by time-resolved fluorescence. For [16]CNB **2**, monitoring the decay of the emission either at the narrow 478 nm or at the broad 526 nm band resulted in almost identical single exponential decay curves ($\tau_{478} = 9.7$ ns, $\tau_{526} = 10.4$ ns), whereas τ_{526} was lengthened to 20.5 ns at 10 K (see SI). Together with the quantum yield at rt ($\Phi_f = 0.13$ in CH_2Cl_2), the intrinsic radiative decay rate can be determined as $k_r = 1.3 \times 10^7 \text{ s}^{-1}$ (for the kinetic model, see SI). [24]CNB **3** exhibits similar recombination properties ($\tau = 10.6$ ns; $\Phi_f = 0.10$; $k_r = 1.0 \times 10^7 \text{ s}^{-1}$), and these rates are approximately one order of magnitude higher than that of **1** ($k_r = 1.5 \times 10^6 \text{ s}^{-1}$).

To clarify the size-dependency of the photophysical properties of these CNBs, (TD-)DFT calculation were carried out at the B3LYP/6-31G(d) level of theory. The energy levels of the frontier molecular orbitals of **1–3** are shown in Figure 3g. The HOMO and LUMO of **1** are delocalized over the central hexagonal rings, while HOMO–1 and LUMO+1 reside predominantly on the ethylene bridges. Similar to CPPs, the HOMO-LUMO gap of CNBs increases with increasing size of the CNBs, which is consistent with the hypsochromic shifts of the absorption and fluorescence spectra of CNBs. The HOMO is stabilized while the HOMO–1 is destabilized with decreasing “bending effect”^{8a} so that the HOMO and HOMO–1 of **2** become close. Furthermore, due to the stabilization and destabilization effects, the orbital corresponding to the HOMO of **1** and **2** becomes the HOMO–1 in the case of **3**, whereby the HOMO of **3** exhibits the same symmetry of the HOMO–1 of **1** and **2**. Accordingly, the $S_0 \rightarrow S_1$ (HOMO \rightarrow LUMO) transitions of **1** and **2** are symmetry forbidden, while that of **3** is symmetry allowed. In the case of **2**, two energetically close transitions exist, *i.e.*, the forbidden $S_0 \leftarrow S_1$ and the allowed $S_0 \leftarrow S_2$, which possibly causes the two-component emission. We then optimized the excited states of **1–3** to simulate the emission spectra (see SI for detail).²⁸ As shown in Figure 3f, the broad emission bands of **1** and **2** fit the symmetry forbidden $S_0 \leftarrow S_1$ transitions, and the sharp peaks of **2** and **3** are also well reproduced by the corresponding symmetry allowed ones ($S_0 \leftarrow S_2$ of **2** and $S_0 \leftarrow S_1$ of **3**); the energy of the 0–0 transitions were rescaled empirically and suitable line widths (700 cm^{-1} and 300 cm^{-1} for the symmetry

forbidden and allowed bands, respectively) were used to match the experimental spectra. Thus, we concluded that the significant size-dependency of the photophysical properties of CNBs, *i.e.*, the broad emission of **1**, the two-component emission of **2**, and the sharp blue fluorescence of **3**, is due to the size-dependent energy shift of the HOMO and HOMO–1 orbitals.

Finally, the Raman spectra of the larger CNBs **2** and **3** were recorded. For **1**, the vibrational modes could be allocated by comparison with the calculated spectrum (see SI), allowing the determination of the fully symmetrical radical breathing mode (RBM) at 217 cm^{-1} (**2**) and 193 cm^{-1} (**3**). The RBM mode of **2** displays almost the same RBM frequency as that of (8,8)CNTs (219 cm^{-1}).²⁹

Conclusions

[12]CNB **1** can now be synthesized in 0.8% overall yield from *p*-xylene, and this route has recently been used on a pilot scale.³⁰ Extending the synthetic strategy to the preparation of the larger [16]CNB **2** and [24]CNB **3** has allowed studying some size-dependent properties and establishing key differences between such CNBs. In particular, the symmetry allowed transition of **3** leads to an exceptionally narrow emission with a full width at half maximum of 270 cm^{-1} (6 nm), which demonstrates that such compounds may represent emitters with very high color purity, a feature that is particularly desirable for optoelectronic materials.³¹ Understanding the effect of the ring-fusion pattern of the CNBs should thus lead to exciting discoveries in this area. Even though this might still be a long-term goal, the synthesis of analogues that exhibit a length/diameter ratio above unity should be the next milestone on the way to unify nanocarbon molecules and allotropes.

ASSOCIATED CONTENT

Supporting Information

The Supporting Information is available free of charge on the ACS Publications website.

Synthetic procedures, characterization data, details of the photophysical measurements, Cartesian coordinates of the optimized structures and NMR spectra of new compounds (PDF)

X-ray crystallographic data for **1**-2THF, **2**, **3**, (*Z,Z,Z,Z*)-**19**, (*Z,Z,Z,E*)-**19**, **20**, and **4-tb** (CIF)

AUTHOR INFORMATION

Corresponding Author

*E-mail: ysegawa@nagoya-u.jp (Y.S.).

*E-mail: itami@chem.nagoya-u.ac.jp (K.I.).

ORCID

Yasutomo Segawa: 0000-0001-6439-8546

Taishi Nishihara: 0000-0001-6973-2005

Yuhei Miyachi: 0000-0002-0945-0265

Kenichiro Itami: 0000-0001-5227-7894

Notes

The authors declare no competing financial interest.

ACKNOWLEDGMENT

This work was supported by the ERATO program from JST (JPMJER1302 to K.I.), the Funding Program for KAKENHI from MEXT (16K05771 to Y.S.), a grant-in-aid for Scientific Research on Innovative Areas “ π -Figuration” (17H05149 to Y.S.), and the Noguchi

Institute (to Y.S.). We thank RIGAKU Co. for the X-ray analysis of **2** and **3**. Calculations were performed using the resources of the Research Center for Computational Science, Okazaki, Japan. ITbM is supported by the World Premier International Research Center Initiative (WPI), Japan.

REFERENCES

- (1) Iijima, S. *Nature* **1991**, *354*, 56.
- (2) (a) Dresselhaus, M.; Dresselhaus, G.; Avouris, P. *Carbon Nanotubes: Synthesis Properties, Applications*, Springer, Berlin, 2001. (b) Dresselhaus, M. S.; Dresselhaus, G.; Saito, R. *Carbon* **1995**, *33*, 883.
- (3) (a) Ajayan, P. M. *Chem. Rev.* **1999**, *99*, 1787. (b) Liu, B.; Wu, F.; Gui, H.; Zheng, M.; Zhou, C. *ACS Nano* **2017**, *11*, 31.
- (4) (a) Segawa, Y.; Ito, H.; Itami, K. *Nat. Rev. Mater.* **2016**, *1*, 15002. (b) Segawa, Y.; Yagi, A.; Matsui, K.; Itami, K. *Angew. Chem. Int. Ed.* **2016**, *55*, 5136.
- (5) Segawa, Y.; Yagi, A.; Ito, H.; Itami, K. *Org. Lett.* **2016**, *18*, 1430.
- (6) Parekh, V. C.; Guha, P. C. *J. Indian Chem. Soc.* **1934**, *11*, 95.
- (7) (a) Yamago, S.; Kayahara, E.; Iwamoto, T. *Chem. Rec.* **2014**, *14*, 84. (b) Golder, M. R.; Jasti R. *Acc. Chem. Res.* **2015**, *48*, 557. (c) Darzi, E. R.; Jasti, R. *Chem. Soc. Rev.* **2015**, *44*, 6401. (d) Lewis, S. E. *Chem. Soc. Rev.* **2015**, *44*, 2221.
- (8) (a) Segawa, Y.; Fukazawa, A.; Matsuura, S.; Omachi, H.; Yamaguchi, S.; Irle, S.; Itami, K. *Org. Biomol. Chem.* **2012**, *10*, 5979. (b) Fujitsuka, M.; Cho, D. W.; Iwamoto, T.; Yamago, S.; Majima, T. *Phys. Chem. Chem. Phys.* **2012**, *14*, 14585. (c) Nishihara, T.; Segawa, Y.; Itami, K.; Kanemitsu, Y. *Chem. Sci.* **2014**, *5*, 2293. (d) Talipov, M.; Jasti, R.; Rathore, R. *J. Am. Chem. Soc.* **2015**, *137*, 14999.
- (9) (a) Kubota, N.; Segawa, Y.; Itami, K. *J. Am. Chem. Soc.* **2015**, *137*, 1356. (b) Kayahara, E.; Patel, V. K.; Mercier, A.; Kundig, P.; Yamago, S. *Angew. Chem., Int. Ed.* **2016**, *55*, 302. (c) Kayahara, E.; Fukayama, K.; Nishinaga, T.; Yamago, S. *Chem. Asian J.* **2016**, *11*, 1793. (d) Kayahara, E.; Qu, R.; Yamago, S. *Angew. Chem. Int. Ed.* **2017**, *56*, 10428.
- (10) (a) Iwamoto, T.; Watanabe, Y.; Sadahiro, T.; Haino, T.; Yamago, S. *Angew. Chem., Int. Ed.* **2011**, *50*, 8342. (b) Iwamoto, T.; Watanabe, Y.; Takaya, H.; Haino, T.; Yasuda, N.; Yamago, S. *Chem. Eur. J.* **2013**, *19*, 14061. (c) Nakanishi, Y.; Omachi, H.; Matsuura, S.; Miyata, Y.; Kitaura, R.; Segawa, Y.; Itami, K.; Shinohara, H. *Angew. Chem., Int. Ed.* **2014**, *53*, 3102. (d) Alvarez, M. P.; Burrezo, P. M.; Kertesz, M.; Iwamoto, T.; Yamago, S.; Xia, J.; Jasti, R.; Navarrete, J. T. L.; Taravillo, M.; Baonza, V. G.; Casado, J. *Angew. Chem., Int. Ed.* **2014**, *53*, 7033. (e) Iwamoto, T.; Slanina, Z.; Mizorogi, N.; Guo, J.; Akasaka, T.; Nagase, S.; Takaya, H.; Yasuda, N.; Kato, T.; Yamago, S. *Chem. Eur. J.* **2014**, *20*, 14403. (f) Alvarez, M. P.; Burrezob, P. M.; Iwamoto, T.; Taravillo, M.; Baonza, V. G.; Navarrete, J. T. L.; Yamago, S.; Casado, J. *Faraday Discuss.* **2014**, *173*, 157. (g) Ueno, H.; Nishihara, T.; Segawa, Y.; Itami, K. *Angew. Chem., Int. Ed.* **2015**, *54*, 3707. (h) Sakamoto, H.; Fujimori, T.; Li, X.; Kaneko, K.; Kan, K.; Ozaki, N.; Hijikata, Y.; Irle, S.; Itami, K. *Chem. Sci.* **2016**, *7*, 4204. (i) Hashimoto, S.; Iwamoto, T.; Kurachi, D.; Kayahara, E.; Yamago, S. *ChemPlusChem* **2017**, *82*, 1015. (j) Ozaki, N.; Sakamoto, H.; Nishihara, T.; Fujimori, T.; Hijikata, Y.; Kimura, R.; Irle, S.; Itami, K. *Angew. Chem. Int. Ed.* **2017**, *56*, 11196. (k) Fukushima, T.; Sakamoto, H.; Tanaka, K.; Hijikata, Y.; Irle, S.; Itami, K. *Chem. Lett.* **2017**, *46*, 855.
- (11) Omachi, H.; Nakamura, T.; Takahashi, E.; Segawa, Y.; Itami, K. *Nat. Chem.* **2013**, *5*, 572.
- (12) Heilbronner, E. *Helv. Chim. Acta* **1954**, *37*, 921.
- (13) Vögtle, F. *Top. Curr. Chem.* **1983**, *115*, 157.
- (14) (a) Vögtle, F.; Schröder, A.; Karbach, D. *Angew. Chem. Int. Ed. Engl.* **1991**, *30*, 575. (b) Friederich, R.; Nieger, M.; Vögtle, F. *Eur. J. Inorg. Chem.* **1993**, *126*, 1723. (c) Kohnke, F. H.; Slawin, A. M. Z.; Stoddart, J. F.; Williams, D. J. *Angew. Chem. Int. Ed. Engl.* **1987**, *26*, 892.
- (15) Esser, B.; Rominger, F.; Gleiter, R. *J. Am. Chem. Soc.* **2008**, *130*, 6716.
- (16) (a) Nakamura, E.; Tahara, K.; Matsuo, Y.; Sawamura, M. *J. Am. Chem. Soc.* **2003**, *125*, 2834. (b) Matsuo, Y.; Tahara, K.; Sawamura, M.; Nakamura, E. *J. Am. Chem. Soc.* **2004**, *126*, 8725. (c) Li, Y.; Xu, D.; Gan, L. *Angew. Chem. Int. Ed.* **2016**, *55*, 2483.
- (17) (a) Scott, L. T.; Boorum, M. M.; McMahon, B. J.; Hagen, S.; Mack, J.; Blank, J.; Wegner, H.; de Meijere, A. *Science* **2002**, *295*, 1500. (b) Scott, L. T.; Jackson, E. A.; Zhang, Q.; Steinberg, B. D.; Bancu, M.; Li, B. *J. Am. Chem. Soc.* **2012**, *134*, 107.
- (18) (a) Cory, R. M.; McPhail, C. L.; Dikmans, A. J.; Vittal, J. J. *Tetrahedron Lett.* **1996**, *37*, 1983. (b) Cory, R. M.; McPhail, C. L. *Tetrahedron Lett.* **1996**, *37*, 1987. (c) Neudorff, W. D.; Lentz, D.; Anibarro, M.; Schlüter, A. D. *Chem. Eur. J.* **2003**, *9*, 2745. (d) Matsui, K.; Fushimi, M.; Segawa, Y.; Itami, K. *Org. Lett.* **2016**, *18*, 5352.
- (19) (a) Kammermeier, S.; Jones, P. G.; Herges, R. *Angew. Chem. Int. Ed. Engl.* **1996**, *35*, 2669. (b) Scott, L. T. *Angew. Chem. Int. Ed.* **2003**, *42*, 4133. (c) Golling, F. E.; Quernheim, M.; Wagner, M.; Nishiuchi, T.; Müllen, K. *Angew. Chem. Int. Ed.* **2014**, *53*, 1525. (d) Merner, B. L.; Dawe, L. N.; Bodwell, G. J. *Angew. Chem. Int. Ed.* **2009**, *48*, 5487. (e) Kuwatani, Y.; Igarashi, J.-I.; Iyoda, M. *Tetrahedron Lett.* **2004**, *45*, 359. (f) Iyoda, M.; Kuwatani, Y.; Nishinaga, T.; Takase, M.; Nishiuchi, T. Chap. 11. In *Fragments of Fullerenes and Carbon Nanotubes*, Petrukina, M., Scott, L. T., Eds.; John Wiley & Sons, Hoboken NJ, 2012. (g) Golder, M. R.; Colwell, C. E.; Wong, B. M.; Zakharov, L. N.; Zhen, J.; Jasti, R. *J. Am. Chem. Soc.* **2016**, *138*, 6577.
- (20) Sisto, T. J.; Zakharov, L. N.; White, B. M.; Jasti, R. *Chem. Sci.* **2016**, *7*, 3681.
- (21) Golder, M. R.; Zakharov, L. N.; Jasti, R. *Pure Appl. Chem.* **2017**, *89*, 1603.
- (22) Povie, G.; Segawa, Y.; Nishihara, T.; Miyauchi, Y.; Itami, K. *Science* **2017**, *356*, 172.
- (23) (a) Dunne, E. C.; Coyne, É. J.; Crowley, P. B.; Gilheany, D. G. *Tetrahedron Lett.* **2002**, *43*, 2449. (b) Byrne, P. A.; Gilheany, D. G. *J. Am. Chem. Soc.* **2012**, *134*, 9225.
- (24) (a) Ruggli, P.; Brandt, F. *Helv. Chim. Acta* **1944**, *27*, 274. (b) Yang, X.; Liu, D.; Miao, Q. *Angew. Chem. Int. Ed.* **2014**, *53*, 6786.
- (25) For recent examples of the Ni(cod)₂/bipyridyl reagent applied to the synthesis of curved polyaromatic hydrocarbons, see: (a) Myśliwiec, D.; Stępień, M. *Angew. Chem. Int. Ed.* **2013**, *52*, 1713. (b) Kayahara, E.; Patel, V. K.; Yamago, S. *J. Am. Chem. Soc.* **2014**, *136*, 2284. (c) Majewski, M. A.; Lis, T.; Cybińska, J.; Stępień, M. *Chem. Commun.* **2015**, *51*, 15094. (d) Myśliwiec, D.; Kondratowicz, M.; Lis, T.; Chmielewski, P. J.; Stępień, M. *J. Am. Chem. Soc.* **2015**, *137*, 1643. (e) Myśliwiec, D.; Lis, T.; Gregoliński, J.; Stępień, M. *J. Org. Chem.* **2015**, *80*, 6300. (f) Majewski, M. A.; Hong, Y.; Lis, T.; Gregoliński, J.; Chmielewski, P. J.; Cybińska, J.; Kim, D.; Stępień, M. *Angew. Chem. Int. Ed.* **2016**, *55*, 14072.

(26) For a discussion on the mechanisms of emission from higher excited states in organic molecules, see: Itoh, T. *Chem. Rev.* **2012**, *112*, 4541.

(27) For a similar dual emission from two rapidly interconverting excited states, see: Kirchhoff, J. R.; Gamache, R. E., Jr; Blaskie, M. W.; Del Paggio, A. A.; Lengel, R. K.; McMillin, D. R. *Inorg. Chem.* **1983**, *22*, 2380.

(28) For the relevance of the Tamm-Dancoff approximation in TD-DFT calculations applied to vibrationally resolved spectral

simulations, see: Chantzis, A.; Laurent, A. D.; Adamo, C.; Jacquemin, D. *J. Chem. Theory Comput.* **2013**, *9*, 4517.

(29) Háróz, E. H.; Duque, J. G.; Rice, W. D.; Densmore, C. G.; Kono, J.; Doorn, S. K. *Phys. Rev. B* **2011**, *84*, 121403.

(30) 1-2THF is currently commercially available from Tokyo Chemical Industry Co., Ltd. (product no. I1078).

(31) Yuan, F.; Yuan, T.; Sui, L.; Wang, Z.; Xi, Z.; Li, Y.; Li, X.; Fan, L.; Tan, Z. a.; Chen, A.; Jin, M.; Yang, S. *Nat. Commun.* **2018**, *9*, 2249.

